Supporting Information

Regulating Crystallization in Wide-Bandgap Perovskite with Removable Additives for an Expanded Processing Window Contributes to Efficient Tandem Solar Cells

*Guanshui Xie, Huan Li, Jun Fang, Xin Wang, Lin Gan, Nuanshan Huang, Haichen Peng, Xiao Lin, Longbin Qiu**

Shenzhen Key Laboratory of Intelligent Robotics and Flexible Manufacturing Systems, Department of Mechanical and Energy Engineering, SUSTech Energy Institute for Carbon Neutrality, Southern University of Science and Technology, Shenzhen, 518055, China

*Corresponding Author:
E-mail: qiulb@sustech.edu.cn

Experimental Section

Materials

Anhydrous dimethyl sulfoxide (DMSO), dimethylformamide (DMF), chlorobenzene (CB), and ethyl alcohol were procured from Sigma Aldrich. Isopropanol (IPA) was acquired from Aladdin. Aluminum oxide nanoparticles (Al_2O_3, ALO; <50 nm particle size as measured by Dynamic Light Scattering, DLS; 20 wt.% in isopropanol) were obtained from Sigma Aldrich. Lead iodide (PbI_2, 99.99%) and phenyl-C61-butyric acid methyl ester (PCBM) were purchased from Advanced Electron Technology. Tetrakis(dimethylamino)tin(IV) (TDMASn) (99.99%-Sn) and water were sourced from Shanghai Oriphant Co., LTD. Formamidine iodide (FAI) and methylammonium bromide (MABr) were supplied by Greatcell Solar Materials. Cesium iodide (CsI), lead bromide ($PbBr_2$), 4-(7H-dibenzo[c,g]carbazol-7-yl)butyl phosphonic acid ((4PADCB)), Phenethylammonium bromide (PEABr) and C_{60} were acquired from Xi'an Polymer Light Technology. All chemicals were utilized as received.

Preparation of perovskite precursor solution: The precursor solution of 1.02 M $Cs_{0.06}FA_{0.66}MA_{0.28}Pb(I_{0.5}Br_{0.5})_3$ was prepared by dissolving 115.8 mg of FAI, 15.9 mg of CsI, 183.4 mg of PbI_2, 228.4 mg of $PbBr_2$ and 32.0 mg of MABr in 1 mL mixed solvents of DMF and DMSO (v/v = 4:1). The additives DCB, DBrB, and DIB were directly incorporated into the perovskite precursor solution at varying concentrations. The solution was shaken by a Vortex Shaker overnight before use.

Preparation of organic precursor solution: The organic solution was prepared by dissolving PM6:Y6:PCBM (1:1.2:0.1, w/w/w) in chloroform with the concentration of donor fixed at 6.5 mg mL^{-1}. The solution was stirred at room temperature overnight. Before use, 0.5 vol% of 1-chloronaphthalene (Sigma-Aldrich) was added to the solution and stirred at 55 °C for 5 min.

Device fabrication

Single-junction WBG perovskite subcells: The ITO-coated substrates (sheet resistance 12 Ω sq^{-1}) were cleaned in diluted detergent, deionized water, and isopropanol for 20 min, sequentially, and UV-ozone treated for 30 min. The structure of the *p*-i-*n* perovskite subcell is glass/ITO/4PADCB/Al_2O_3/$Cs_{0.06}FA_{0.66}MA_{0.28}Pb(I_{0.5}Br_{0.5})_3$/PCBM/$C_{60}$/ALD SnO_X/Ag. The HTL of 4PADCB (0.4 mg mL^{-1} in ethanol) was spin-coated at 3,000 r.p.m. for 30 s with a ramp of 10 s and annealed at 100 °C for 10 min. The dielectric layer of Al_2O_3 solution was spin-coated on the 4PADCB film at 5,000 r.p.m. for 30 s, and annealed at 100 °C for 10 min. After

filtering the precursor solution through 0.22 μm PTFE, the $Cs_{0.06}FA_{0.66}MA_{0.28}Pb(I_{0.5}Br_{0.5})_3$ perovskite films were then deposited by spin-coating the precursor solution onto 4PADCB/Al_2O_3 films at 1,950 r.p.m. for 20 s, 4,000 r.p.m. for 15-50 s, and 150 μL of CB was slowly dropped after 20-60 s to adjust the appropriate anti-solvent processing times. The films were then immediately annealed at 105 °C for 15 min. After cooling to room temperature, 45 μL of PEABr solution (1.5 mg mL^{-1} in IPA) was quickly dropped on the perovskite film and spin-coated at 5,000 r.p.m. for 30 s, then annealed at 105 °C for 5 min. The electron transport layers were prepared by spin-coating 20 μL PCBM solution (10 mg mL^{-1} in CB) at 2,000 r.p.m. for 30 s and then evaporating 10 nm of C_{60} in a high-vacuum thermal evaporator. After that, ~20 nm (~170 Cycle) of SnO_X was fabricated by atomic layer deposition technique. Finally, 90 nm metal electrode of Ag was subsequently evaporated to complete the device fabrication.

Single-junction organic subcells: The cleaned ITO-coated substrates were UV-ozone treated for 30 min. PEDOT:PSS (Al 4083) diluted into water by 1:1 was sequentially spin-coated onto the as-prepared substrates at 4,000 r.p.m. for 30 s and then annealed at 120 °C for 15 min. After that, the substrates were transferred into an N_2-filled glovebox. The PM6:Y6:PCBM organic films were then deposited by dynamically spin-coating at 2,300 r.p.m. for 55 s. The as-prepared films were annealed immediately under 110 °C for 8 min. After cooling, PDINN (1 mg mL^{-1} in methanol) was drop-cast on top as an *n*-type interfacial layer. Finally, 90 nm Ag was thermally evaporated as a top electrode with a metal shadow mask.

Deposition of SnO_X layer: SnO_X films were deposited by an atomic layer deposition (ALD) technique in an ALD system (Wuhan Pudi). The ALD SnO_X served as the hole block layer in the single-junction devices and the interconnecting layer in the tandem cells. The reacting temperature during the deposition was kept at 100 °C, and TDMASn (at 60 °C) and H_2O (at 25 °C) were used as precursors for SnO_X fabrication. High-purity nitrogen (N_2, 99.999%) was used as carrier gas and purge gas. Chamber and process nitrogen flows were set to 12 and 12 sccm to maintain the chamber pressure at 2.2 torr, respectively. A 20 nm thick SnO_X film was deposited by 170 cycles, achieving 0.12 nm per cycle: TDMASn (pulse time 0.35 s, purge time 15 s) and H_2O (pulse time 0.15 s, purge time 15 s).

Perovskite-organic tandem cells: After deposition of PCBM/C_{60}, the as-prepared WBG perovskite subcells were transferred to an ALD system, where the ~20 nm SnO_X was deposited on top as a barrier layer, and then PEDOT:PSS was spin-coated as an HTL for the organic

subcells. The organic films were deposited by spin-casting at 2,300 r.p.m. for 55 s and immediately annealed at 110 °C for 8 min. After cooling, 30 μL of PDINN was spin-casted on top at 3,000 r.p.m. for 30 s as an electron transport layer. Finally, 90 nm Ag was thermally evaporated as a top electrode.

Device Characterization

The current density versus voltage (*J-V*) characteristics of the PSCs were tested using a Keithley 2420 source meter under AM 1.5G one-sun illumination (100 $mW \cdot cm^{-2}$), which was produced by a solar simulator (Sol3A Class AAA, Oriel, Newport, USA) at room temperature. A standard reference silicon cell (91150-KG3, Newport, USA) was used to calibrate the light intensity. The metal masks with an area of 0.1 cm^2 were employed to determine the active area. The voltage was scan from 1.4 V to -0.1 V for the reverse scan, and from -0.1 V to 1.4 V for the forward scan in WBG PSC. A voltage scan from 1.0 to -0.1 V was applied for the OSCs. The voltage was scanned from 2.22 V to -0.1 V for the reverse scan of the TSCs, and from -0.1 V to 2.22 V for the forward scan of the TSCs. The voltage step in the scan was 15 mV at scan speed 100 $mV\ s^{-1}$. The measurements were performed in ambient air with a humidity of 50-70% and a temperature of 25 °C. The Incident Photon-to-Electron Conversion Efficiency (IPCE) measurement was conducted to obtain the external quantum efficiency (EQE) spectra with a range from 300 to 1000 nm using EQE system (IQE 200B, Newport). The operational stability was tested by a stability measurement system (PURI 2400-8Q), equipped with multiple sample chambers and automatic data-collecting elements. The electroluminescence (EL) spectra were characterized by a Keithley 2420 source meter and integrating sphere connected to a spectrophotometer (QE65Pro, BIAOQI OPTOELECTRONICS). The Electrochemical impedance spectroscopy (EIS) curves of the devices were determined by using an AutoLab electrochemical station with a frequency of 10 Hz to 1 MHz in a dark environment.

Material Characterization

XRD patterns were acquired in the air by using a Rigaku Smartlab with Cu Kα radiation in the 2θ range of 3-60° at a scanning rate of $10°\ min^{-1}$. The wavelength (λ) of the incident X-ray is 1.5418 Å. The photoluminescence (PL) spectra, in-situ PL, and PLQY were performed using an BIAOQI OPTOELECTRONICS system applying a 405 nm laser as the excitation source. The scanning electronic microscope (SEM) images were obtained from Merlin field emission SEM at an acceleration voltage of 2-5 kV and a current of 25-50 pA. The roughness of the films were collected from the atomic force microscope (AFM, MFP-3D Stand Alone). The PL

mapping images were obtained using a laser scanning confocal microscope (Leica, TCS SP8) with a pulsed excitation at 488 nm. The absorption of the films was attained from UV-Vis spectroscopy (HITACHI, UH5700), employing an optical range from 300 to 1000 nm in air.

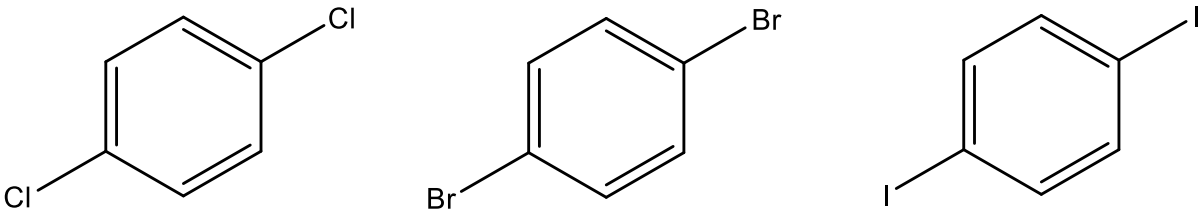

1,4-Dichlorobenzene
mp. 52 ℃
bp. 174 ℃

1,4-Dibromobenzene
mp. 83-87 ℃
bp. 219 ℃

1,4-Diiodobenzene
mp. 131 ℃
bp. 285 ℃

Figure S1. Chemical structures of DCB, DBrB, and DIB used in this work.

Table S1. The melting point and boiling point of the DMF and DMSO compared with the removable additive used in this work.

	Melting point (mp.) ℃	Boiling point (bp.) ℃
DMF	-61	153
DMSO	18.4	189
DCB	52	174
DBrB	83-87	219
DIB	131	285

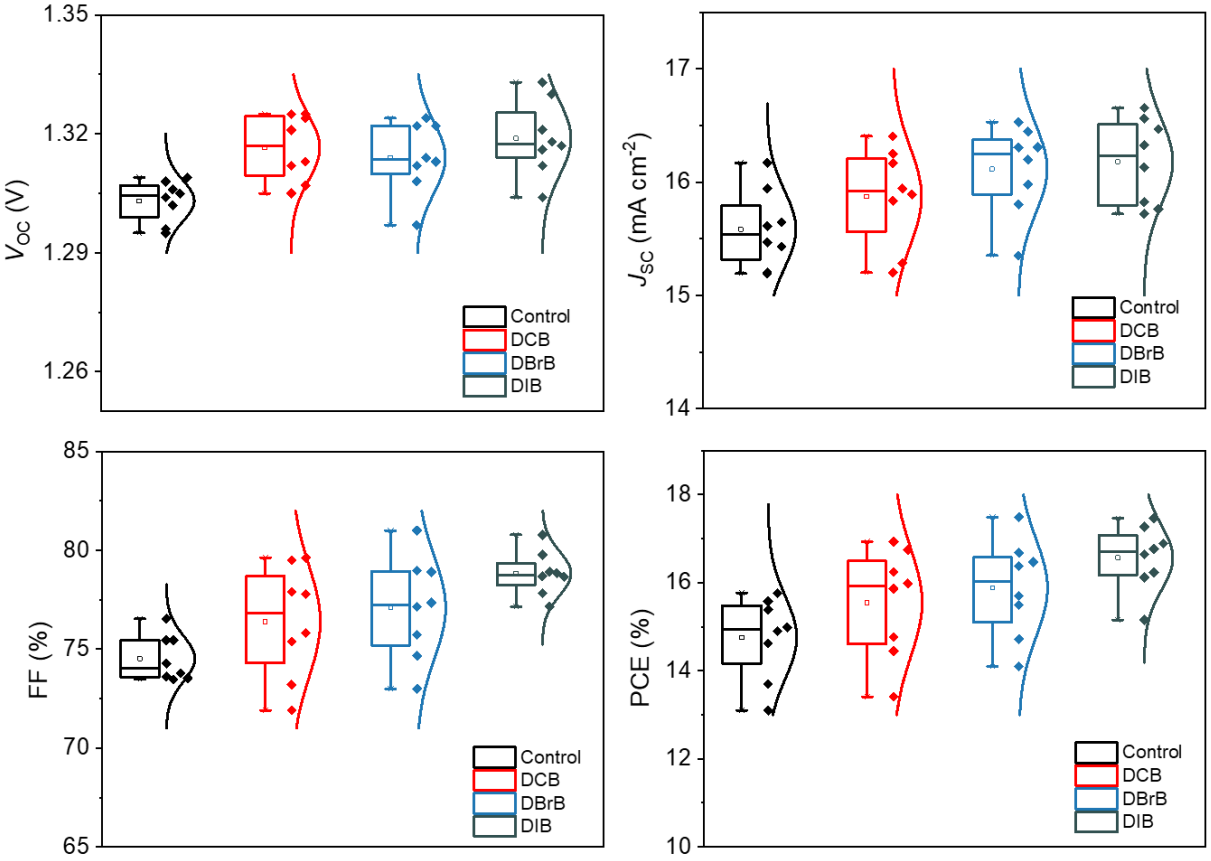

Figure S2. Statistics of V_{OC}, J_{SC}, FF and PCE distribution of WBG PSCs with DCB, DBrB and DIB added in the perovskite precursor (The optimal concentration of these additives was determined to be 3 mg mL^{-1}).

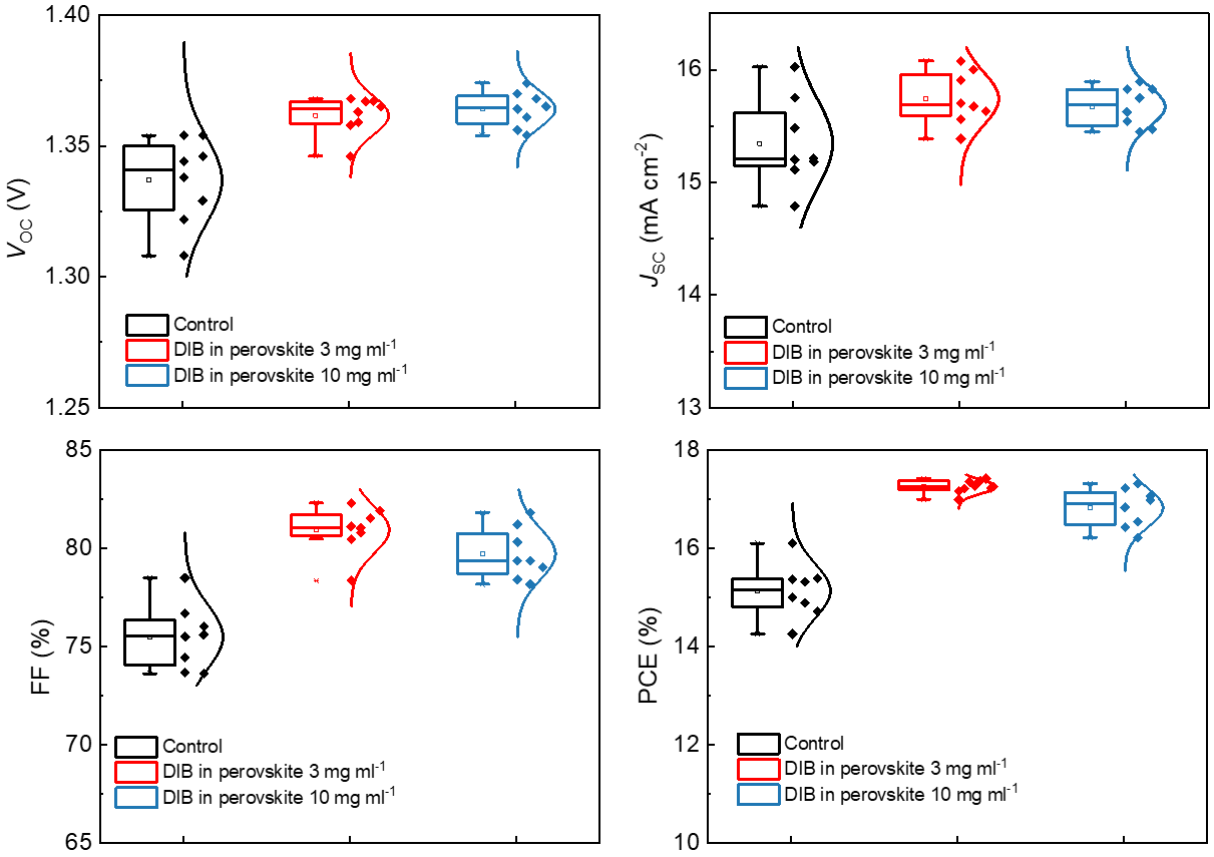

Figure S3. Statistics of V_{OC}, J_{SC}, FF, and PCE distribution of WBG PSCs with different concentrations of DIB added in the perovskite precursor.

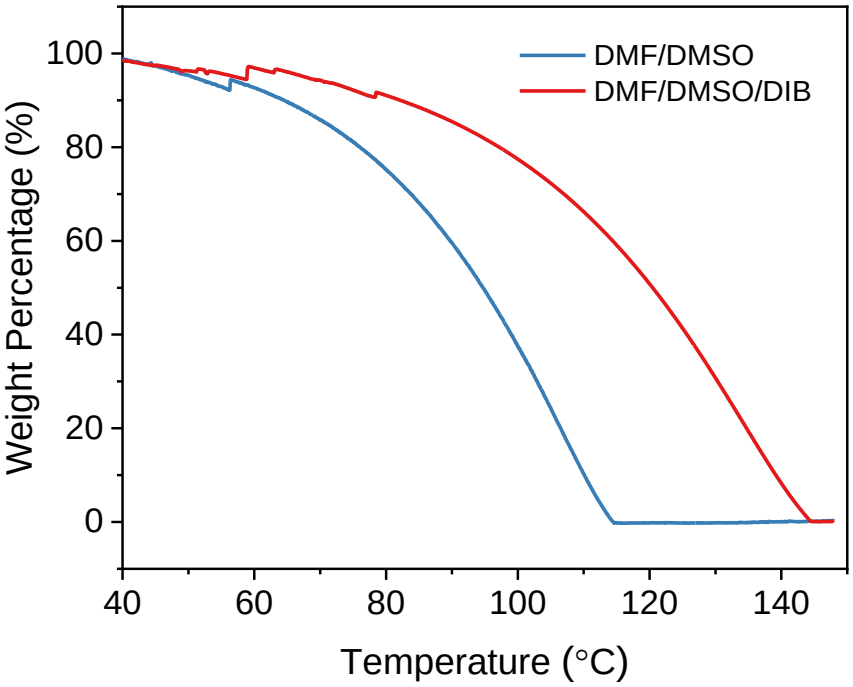

Figure S4. Thermogravimetric analysis (TGA) plot of DMF/DMSO and DMF/DMSO+DIB at a scan rate of 5 °C min^{-1} under an inert atmosphere.

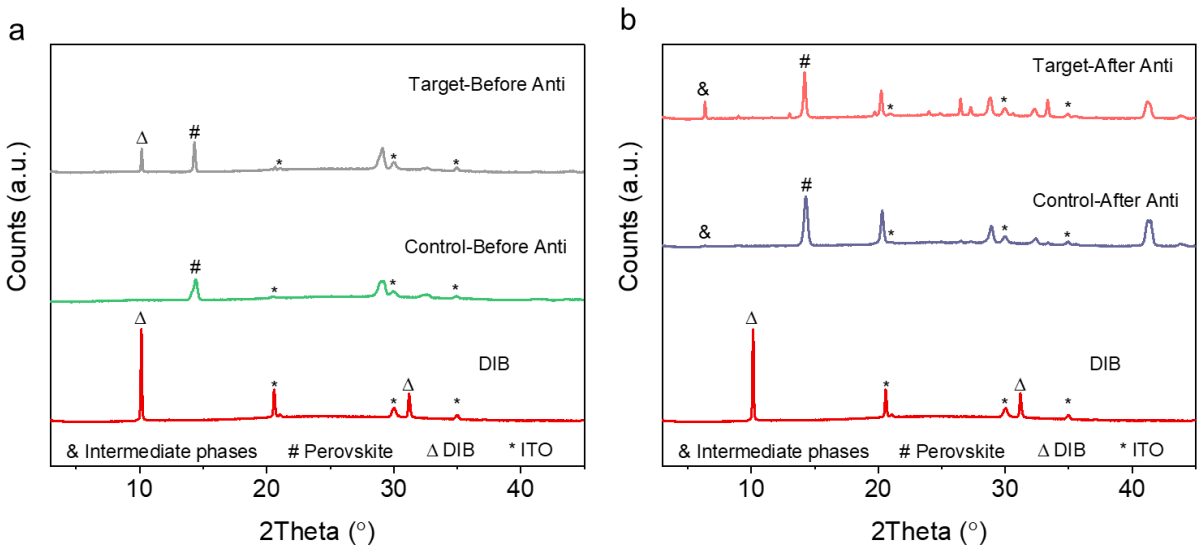

Figure S5. XRD pattern of the perovskite film **a.** before or **b.** after dropping the antisolvent.

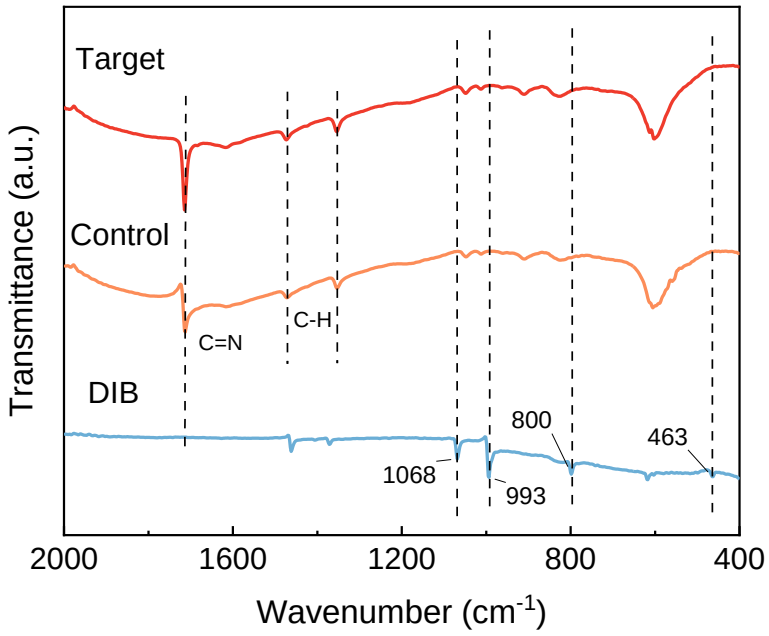

Figure S6. Fourier transform infrared (FTIR) spectra of the control and target perovskite films after annealing.

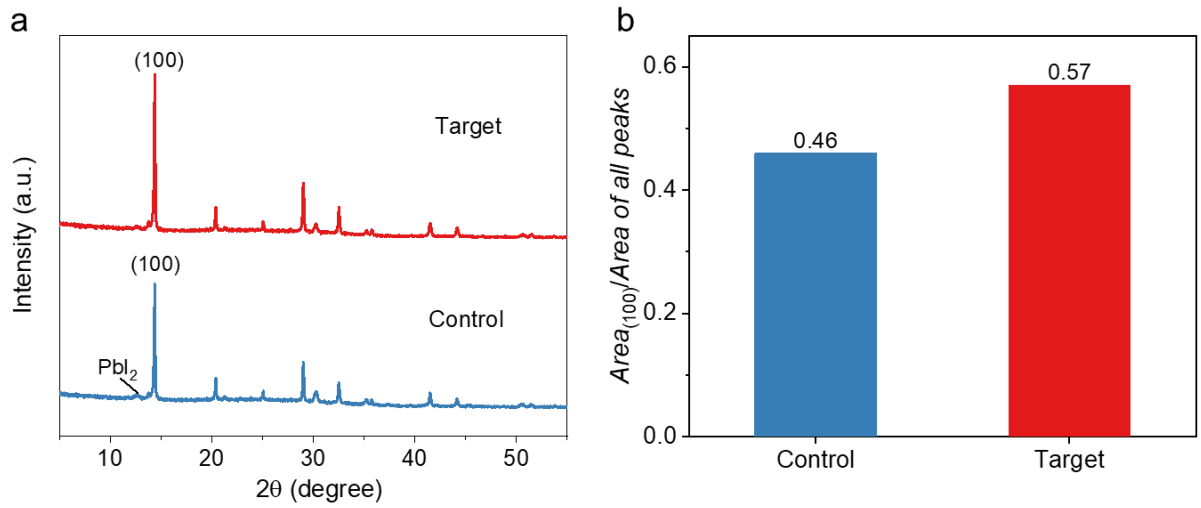

Figure S7. a. XRD patterns of as-deposited perovskite films with or without solid additives of DIB investigated in this study. **b.** The area ratio of perovskite (100) to all of peaks to calculate the crystallinity of perovskite.

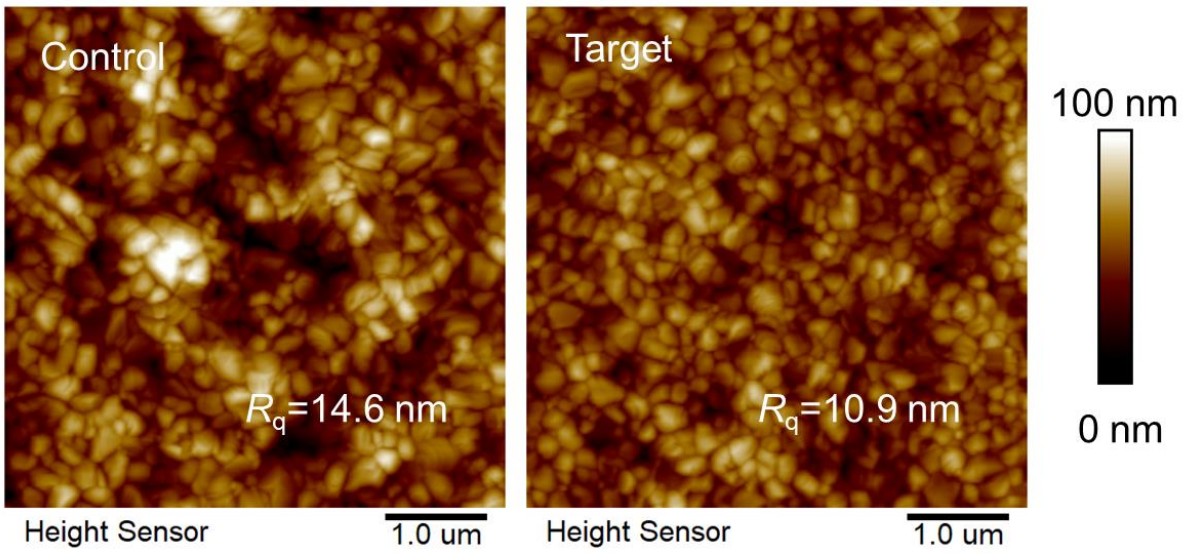

Figure S8. The surface morphology of perovskite films without and with additives.

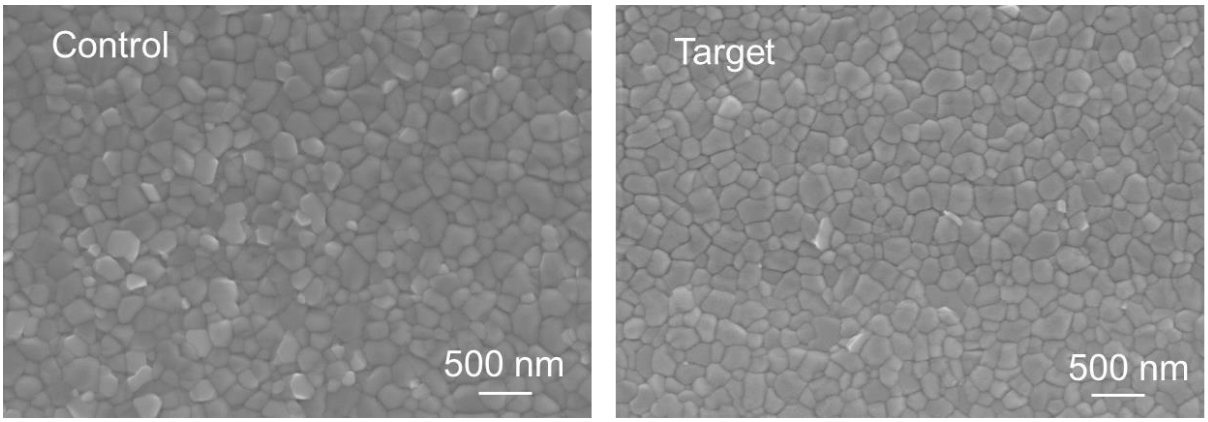

Figure S9. Top-view SEM images of perovskite films without and with DIB.

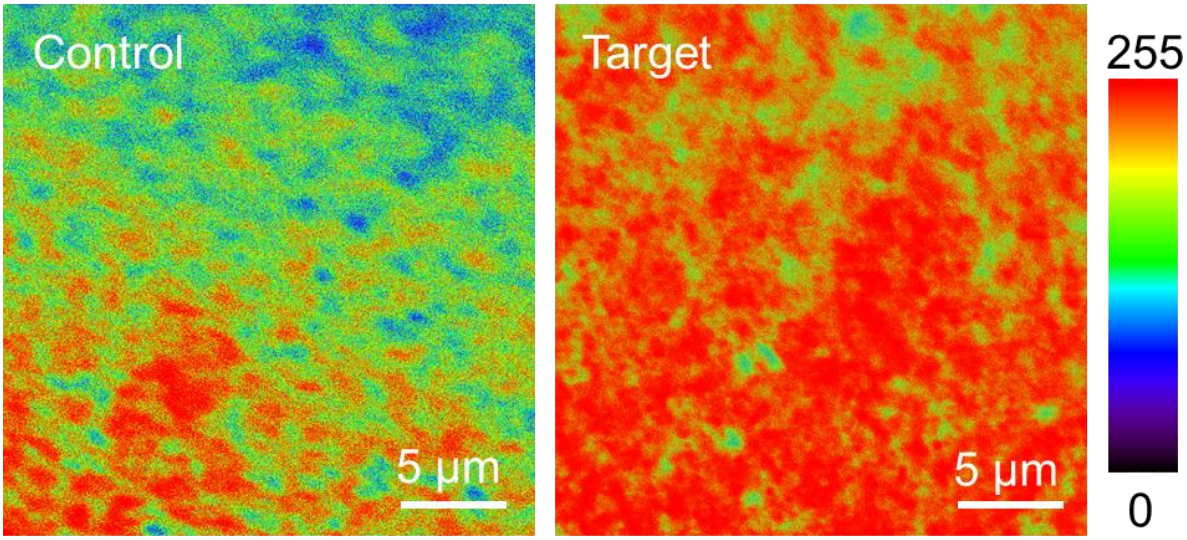

Figure S10. The PL mapping of perovskite films without and with DIB.

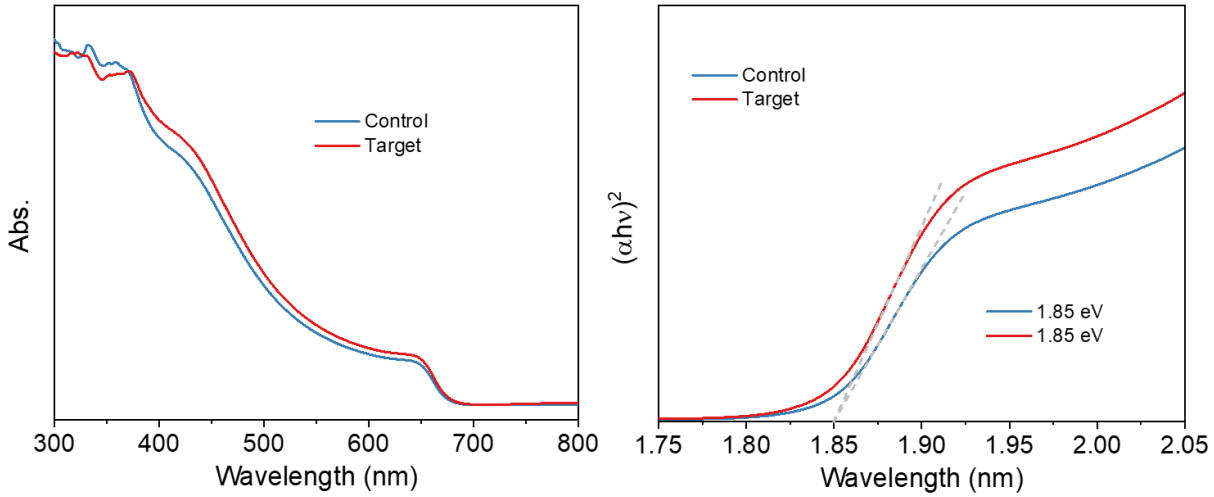

Figure S11. UV-Vis absorption spectra (left) and tauc-plots (right) with fitted optical bandgaps for wide-bandgap perovskites without and with DIB.

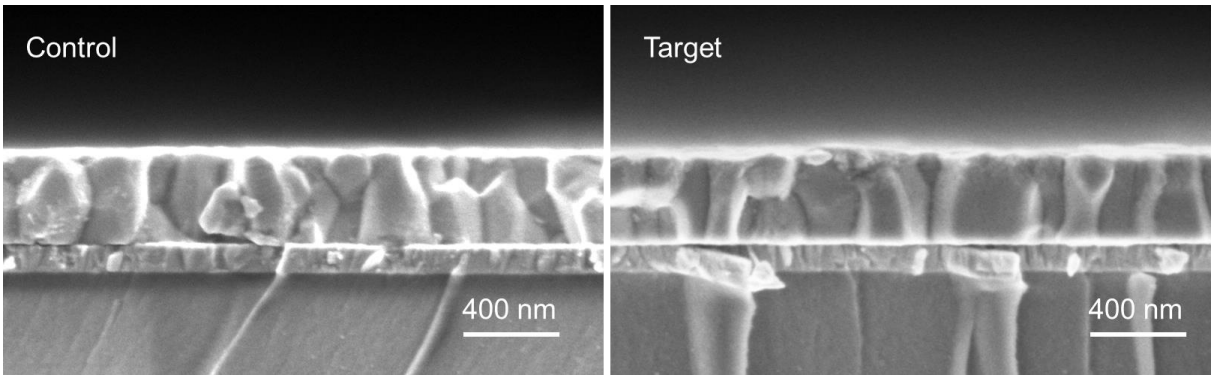

Figure S12. The cross-sectional SEM images of the perovskite films without and with DIB additive.

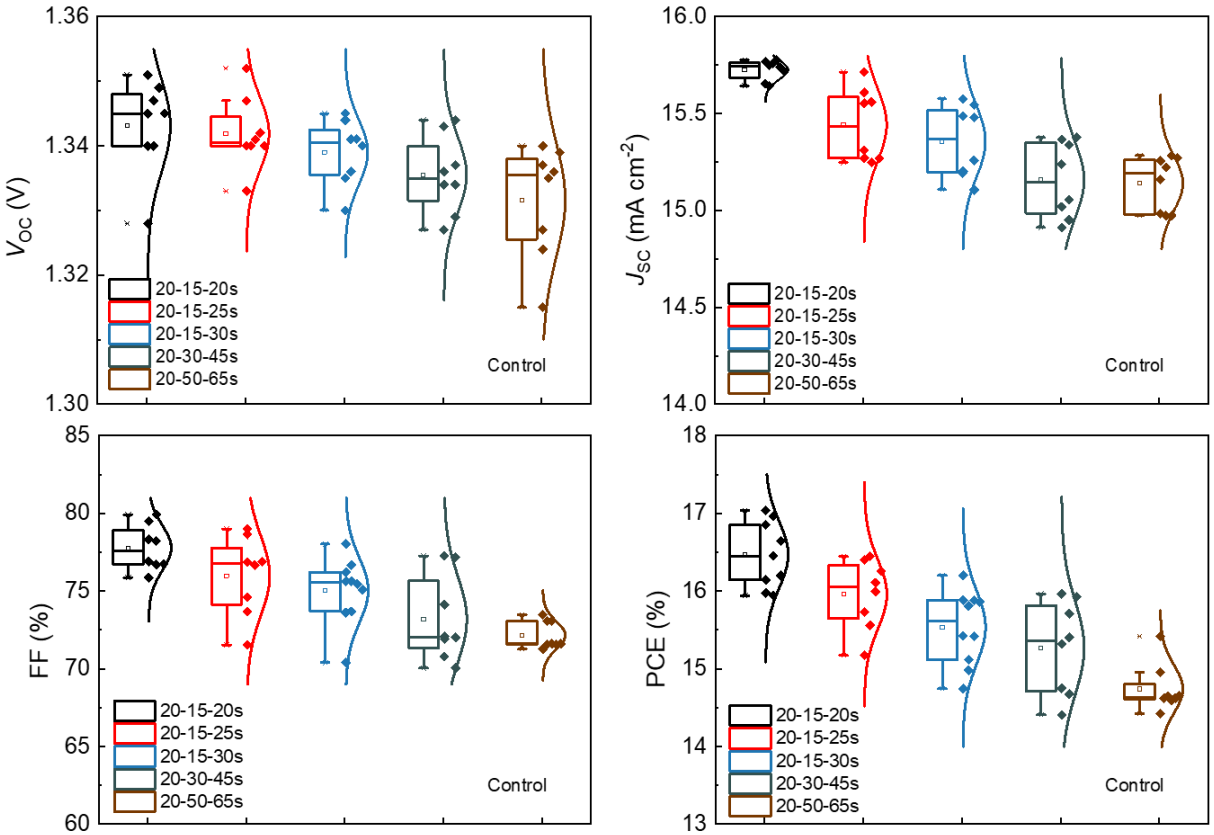

Figure S13. Statistics of V_{OC}, J_{SC}, FF, and PCE distribution of Control WBG PSCs at prolonged dropping anti-solvent times. (e.g. 20-15-20 s indicate the two-step coating process and drop the anti-solvent at start of 20 s.)

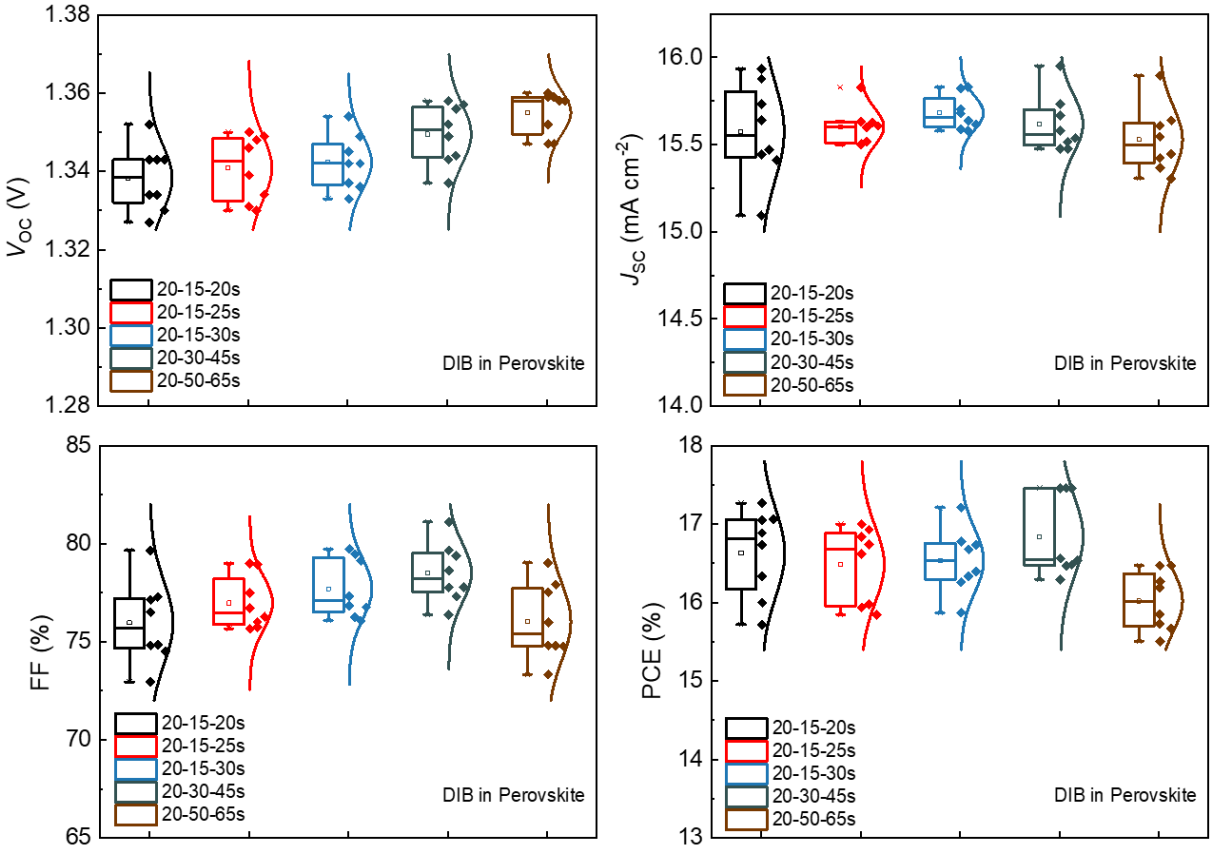

Figure S14. Statistics of V_{OC}, J_{SC}, FF, and PCE distribution of DIB in Perovskite-based WBG PSCs at prolonged dropping anti-solvent times. (e.g. 20-15-20s indicate the two-step coating process and drop the anti-solvent at start of 20 s.)

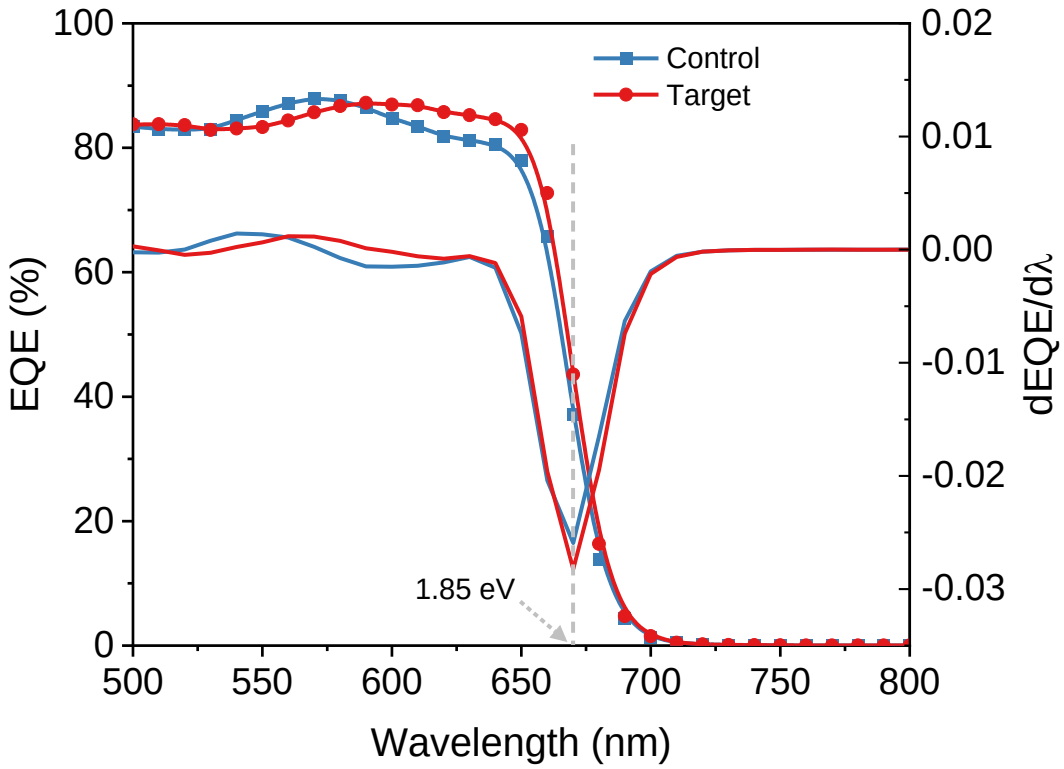

Figure S15. Photovoltaic bandgaps calculated using the inflection points of the EQE curves.

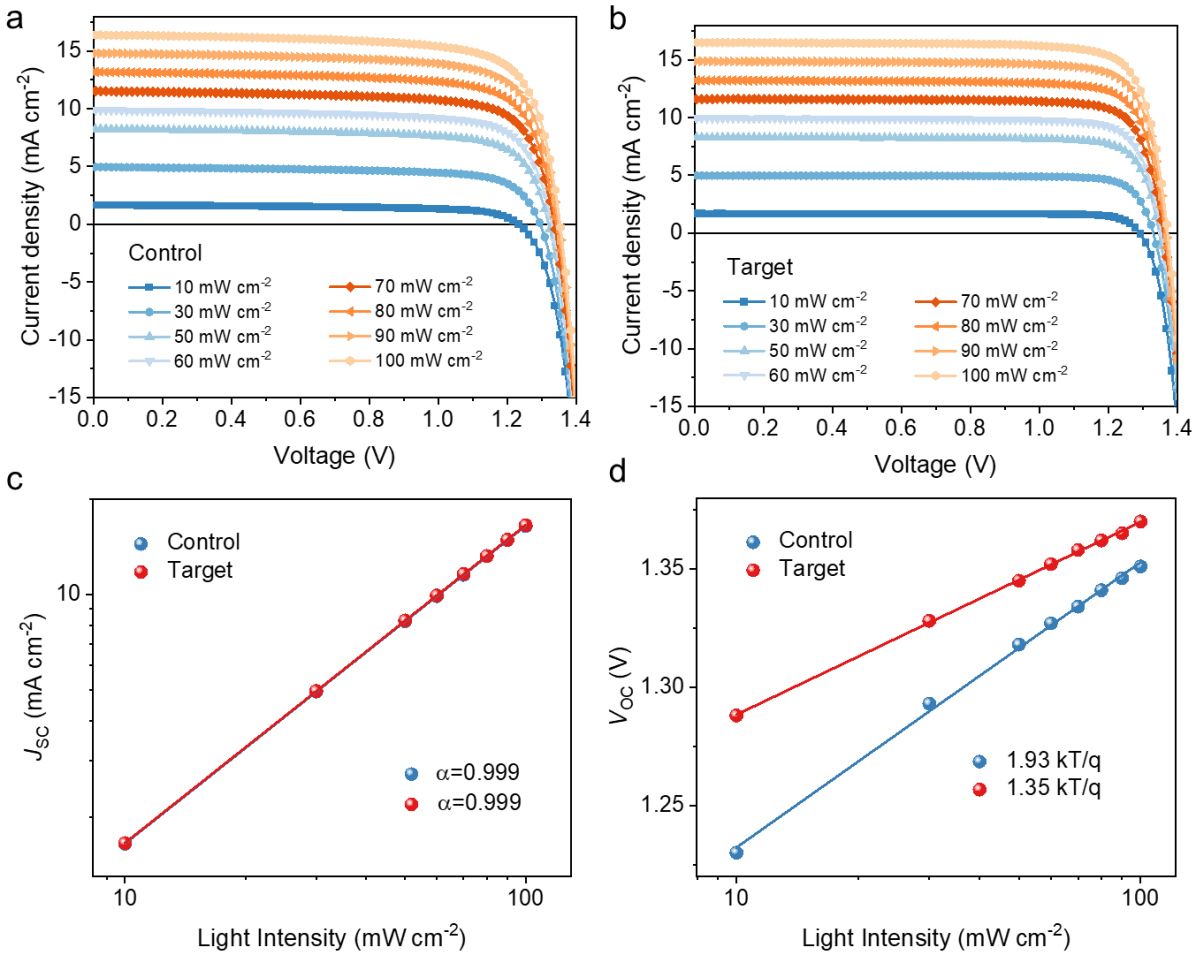

Figure S16. Current-voltage curves of **a.** control and **b.** target device under different light intensities. **c.** Dependeddncy relation of J_{SC} and linght intensity, **d.** dependency relation of V_{OC} and light intensity extract form **a.** and **b.**

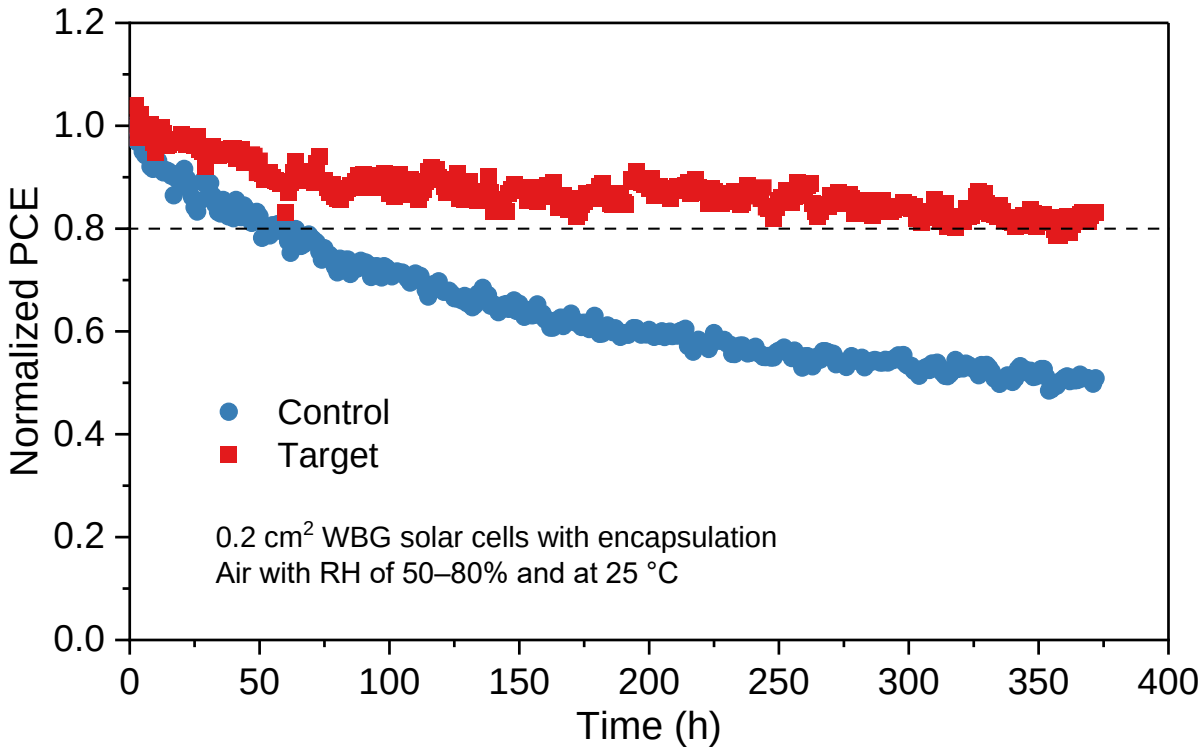

Figure S17. Normalized PCEs under MPP tracking for the WBG PSCs. The devices with encapsulation were measured under 100 mW cm^{-2} illumination with a LED light source.

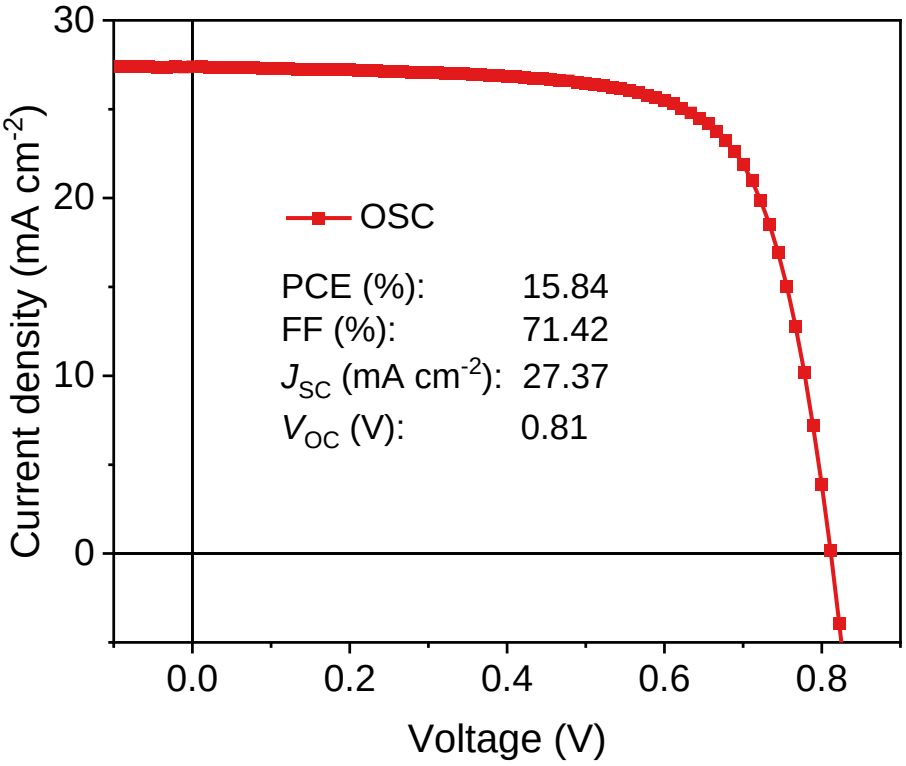

Figure S18. The *J-V* curve and photovoltaic performance of NBG OSC with the structure of ITO/PEDOT:PSS/PM6:Y6:PCBM/Ag.

Table S2. Summary of the photovoltaic performance of WBG PSCs and TSCs in *p*-i-*n* type perovskite-organic TSCs.

Device structure	Year	WBG PSCs photovoltaic parameters					TSCs photovoltaic parameters				Ref.
		E_g (eV)	V_{OC} (V)	J_{SC} (mA cm^{-2})	FF (%)	PCE (%)	V_{OC} (V)	J_{SC} (mA cm^{-2})	FF (%)	PCE (%)	
ITO/PEDOT:PSS/PBSeDTEG8:PCBM/PFN/TiO_2/PEDOT:PSS PH500/PEDOT:PSS 4083/$MAPbI_3$/PCBM/Al	2015	1.5	0.92	14.1	70	9.08	1.52	10.05	67.0	10.23	[1]
ITO/PEDOT:PSS/$MAPbI_3$/$PC_{61}BM$/C_{60}-SB/Ag/MoO_3/PCE-10:$PC_{71}BM$/C_{60}-N/Ag	2016	1.5	1.03	15.6	70.6	11.4	1.63	13.1	75.1	16.0	[2]
ITO/NiO_X/$FA_{0.8}MA_{0.02}Cs_{0.18}PbI_{1.8}Br_{1.2}$/$C_{60}$/BCP/Ag/$MoO_X$/PBDBT-2F:Y6:$PC_{71}BM$/TPBi/Ag	2020	1.77	1.100	16.1	83.1	14.7	1.902	13.05	83.1	20.6	[3]
ITO/Poly-TPD/$MA_{0.9}FA_{0.1}Pbl_2Br(SCN)_{0.12}$/PCBM/BCP/Au/$MoO_3$/PM6:CH1007/PFN-Br/Ag	2022	1.72	1.19	18.7	78.4	17.4	1.96	13.8	78.4	21.2	[4]
ITO/2PACz/$FA_{0.6}MA_{0.4}Pb(I_{0.6}Br_{0.4})_3$/C60/BCP/Ag/MoOX/PTB7-Th:BTPV-4Cl-eC9/PDINN/Ag	2022	1.79	1.25	16.9	83.0	17.6	1.88	15.7	74.6	22.0	[5]
ITO/NiO_X/BPA/$CS_{0.25}FA_{0.75}Pb(I_{0.6}Br_{0.4})_3$/$C_{60}$/BCP/IZO/$MoO_X$/PM6:Y6:$PC_{71}BM$/PNDIT-F3N/Ag	2022	1.79	1.26	17.90	78.9	17.80	2.06	14.83	77.2	23.6	[6]
ITO/PTAA/$FA_{0.8}CS_{0.2}Pb(I_{0.5}Br_{0.5})_3$/$SnO_X$/$InO_X$/$MoO_X$/PM6:Y6:$PC_{61}BM$/$C_{60}$/BCP/Ag	2022	1.85	1.34	15.6	81	16.8	2.15	14.0	80.0	24.0	[7]
ITO/MeO-2PACz/$FA_{0.6}MA_{0.4}Pb(I_{0.6}Br_{0.4})_3$/PCBM/$SnO_X$/PED/PM6:Y6/PDINN/Ag	2023	1.77	1.33	16.43	80.94	17.72	2.12	14.08	74.95	22.31	[8]
ITO/MeO-2PACz/$FA_{0.8}Cs_{0.2}Pb(I_{0.6}Br_{0.4})_3$/$C_{60}$/C-C1-P/Ag/$MoO_X$/PM6:BTP-eC9:$PC_{71}BM$/TPMA/Ag	2023	1.77	1.24	17.93	81.44	18.05	2.09	14.58	78.99	24.07	[9]
ITO/4PADCB/$FA_{0.8}MA_{0.1}Cs_{0.1}Pb(I_{0.5}Br_{0.5})_3$/$C_{60}$/$SnO_2$/Au/$MoO_X$/PM6:BTP-eC9:PCBM/PNDIT-F3N/Ag	2023	1.85	1.36	16.21	83.21	18.14	2.197	14.15	77.6	24.12	[10]
ITO/NiO_X/2PACz/$FA_{0.8}Cs_{0.2}Pb(I_{0.5}Br_{0.5})_3$/$C_{60}$/BCP/Au/$MoO_X$/PM6:PM7:Y6:$PC_{71}BM$/$C_{60}$/BCP/Ag	2023	1.85	1.35	16.78	83.29	18.87	2.14	14.17	80.71	24.47	[11]
ITO/DC-PA/$Cs_{0.2}FA_{0.8}Pb(I_{0.6}Br_{0.4})_3$/$C_{60}$/BCP/Au/$MoO_X$/PM6:Y6:$PC_{71}BM$/PNDIT-F3N/Ag	2024	1.81	1.351	17.52	82.74	19.58	2.151	14.36	81.65	25.22	[12]
ITO/4PADCB/$FAMACsPb(I_{0.5}Br_{0.5})_3$/PCBM/$C_{60}$/$SnO_X$/Au/PED/PM6:Y6:PCBM/PDINN/Ag	2024	1.85	1.370	15.45	81.81	17.32	2.147	13.87	79.08	23.55	This work

References

[1] C.-C. Chen, S.-H. Bae, W.-H. Chang, Z. Hong, G. Li, Q. Chen, H. Zhou, Y. Yang, *Mater. Horiz.* **2015**, 2, 203.

[2] Y. Liu, L. A. Renna, M. Bag, Z. A. Page, P. Kim, J. Choi, T. Emrick, D. Venkataraman, T. P. Russell, *ACS Appl. Mater. Interfaces* **2016**, 8, 7070.

[3] X. Chen, Z. Jia, Z. Chen, T. Jiang, L. Bai, F. Tao, J. Chen, X. Chen, T. Liu, X. Xu, C. Yang, W. Shen, W. E. I. Sha, H. Zhu, Y. Yang, *Joule* **2020**, 4, 1594.

[4] Y. M. Xie, Q. Yao, Z. Zeng, Q. Xue, T. Niu, R. Xia, Y. Cheng, F. Lin, S. W. Tsang, A. K. Y. Jen, H. L. Yip, Y. Cao, *Adv. Funct. Mater.* **2022**, 32, 2112126.

[5] S. Qin, C. Lu, Z. Jia, Y. Wang, S. Li, W. Lai, P. Shi, R. Wang, C. Zhu, J. Du, J. Zhang, L. Meng, Y. Li, *Adv. Mater.* **2022**, 34, 2108829.

[6] W. Chen, Y. Zhu, J. Xiu, G. Chen, H. Liang, S. Liu, H. Xue, E. Birgersson, J. W. Ho, X. Qin, J. Lin, R. Ma, T. Liu, Y. He, A. M.-C. Ng, X. Guo, Z. He, H. Yan, A. B. Djurišić, Y. Hou, *Nat. Energy* **2022**, 7, 229.

[7] K. O. Brinkmann, T. Becker, F. Zimmermann, C. Kreusel, T. Gahlmann, M. Theisen, T. Haeger, S. Olthof, C. Tückmantel, M. Günster, T. Maschwitz, F. Göbelsmann, C. Koch, D. Hertel, P. Caprioglio, F. Peña-Camargo, L. Perdigón-Toro, A. Al-Ashouri, L. Merten, A. Hinderhofer, L. Gomell, S. Zhang, F. Schreiber, S. Albrecht, K. Meerholz, D. Neher, M. Stolterfoht, T. Riedl, *Nature* **2022**, 604, 280.

[8] G. Xie, H. Li, X. Wang, J. Fang, D. Lin, D. Wang, S. Li, S. He, L. Qiu, *Adv. Funct. Mater.* **2023**, 33, 2308794.

[9] Z. Ma, Y. Dong, R. Wang, Z. Xu, M. Li, Z. a. Tan, *Adv. Mater.* **2023**, 35, 2307502.

[10] Y. An, N. Zhang, Z. Zeng, Y. Cai, W. Jiang, F. Qi, L. Ke, F. R. Lin, S. W. Tsang, T. Shi, A. K. Y. Jen, H. L. Yip, *Adv. Mater.* **2023**, 36, 2306568.

[11] X. Wang, D. Zhang, B. Liu, X. Wu, X. Jiang, S. Zhang, Y. Wang, D. Gao, L. Wang, H. Wang, Z. Huang, X. Xie, T. Chen, Z. Xiao, Q. He, S. Xiao, Z. Zhu, S. Yang, *Adv. Mater.* **2023**, 35, 2305946.

[12] S. Wu, Y. Yan, J. Yin, K. Jiang, F. Li, Z. Zeng, S.-W. Tsang, A. K. Y. Jen, *Nat. Energy* **2024**, 9, 411.